Vertical distribution and migration of mesopelagic scatterers in four north Atlantic basins

Thor A. Klevjer [a,*], Webjørn Melle [a], Tor Knutsen [a], Dag Lorents Aksnes [b]

[a] Institute of Marine Reseach, Bergen, Norway
[b] Department of Biological Sciences, University of Bergen, Bergen, Norway

ABSTRACT

We studied vertical distribution and diel vertical migration (DVM) behaviour of mesopelagic acoustic scattering layers in relation to environmental conditions in the Norwegian Sea, the Iceland Sea, the Irminger Sea, and the Labrador Sea. Distinct mesopelagic scattering layers were found in all basins, but the daytime depth of the layers varied between basins. The results suggested that daytime vertical distribution across the four basins are strongly influenced by optical conditions. DVM occurred in all basins, and since daytime vertical distribution was influenced by optical conditions, it affected the amplitude of vertical connectivity. We used the proportion of the acoustic backscatter that migrated vertically into the epipelagic zone as a proxy for active vertical flux to the mesopelagic. The proportion of micronekton backscatter participating in the vertical migrations varied between the basins, with the highest and lowest vertical connectivity in the Norwegian Sea and the Iceland Sea respectively. We conclude that a more than 8-fold reduction in backscatter flux in the Iceland Sea was primarily attributable to optical conditions there, as high nighttime light levels appeared to exclude the micronekton from the epipelagic zone.

1. Introduction

The connectivity between the upper and the lower ocean is strongly influenced by patterns of vertical biomass structure and involve animals performing interzonal DVM. Accumulated scientific evidence suggest that the mesopelagic domain is home to a large biomass of organisms (Gjøsæter and Kawaguchi, 1980; Kaartvedt et al., 2012; Irigoien et al., 2014). As primary production at mesopelagic depths is nil, the vertical transport of energy (organic carbon) to these depths must be an important factor structuring mesopelagic ecosystems (Sutton, 2013). Many of the mesopelagic organisms perform diel vertical migrations, thereby contributing to vertical fluxes of carbon and nutrients, while others are permanent residents of mesopelagic depths and rely on carbon and energy being transported to their vertical horizon. Some studies have concluded that the contribution of mesopelagic organisms to overall vertical transport of carbon is relatively small (Longhurst and Glen Harrison, 1989), while other studies suggest that the fish-mediated carbon flux to the deep sea is potentially huge (Davison et al., 2013; Irigoien et al., 2014; Klevjer et al., 2016). While the contribution of mesozooplankton to the active carbon transport has been fairly well studied (Steinberg et al., 2000; Hernandez-Leon et al., 2010) the contribution from micronektonic mesopelagic organisms is largely a black box, with global quantification still in its infancy (Irigoien et al., 2014; Klevjer et al., 2016; Aumont et al., 2018). While a large portion of

this uncertainty is caused by uncertainties in mesopelagic biomasses (Kaartvedt et al., 2012; Irigoien et al., 2014; Proud et al., 2018), increased knowledge of large-scale patterns in migratory behaviour (Klevjer et al., 2016) and amplitudes (Bianchi et al., 2013) are also required to determine the fish-mediated carbon flux.

Our current ecological basis for the open ocean vertical zonation scheme are light-levels (Sutton, 2013), and both early and recent studies of vertical structures in mesopelagic scattering layers have found strong relationships between vertical biomass patterns and light penetration (Kampa, 1971; Dickson, 1972; Aksnes et al., 2017). However, oxygen, temperature and other environmental factors also correlate with the vertical connectivity through e.g. their influence on migratory behaviour, which varies extensively globally (Bianchi et al., 2013; Klevjer et al., 2016). Although light forms the basis for the oceanic vertical zonation scheme and has a pivotal role in shaping vertical structure of life in the oceans, light characterization is seldom made in mesopelagic studies (but see Kampa, 1971; Widder et al., 1992; Aksnes et al., 2017). Here, variables such as salinity, temperature and oxygen are more often reported. Since vertical structure and behaviour do correlate with these variables (Bianchi et al., 2013; Klevjer et al., 2016), they are potential explanatory variables. The lack of direct observations of light at depth, which is known as the main proximate cue for DVM behaviour and thereby active vertical flux, is unfortunate (Kaartvedt et al., 2019). Here, we use observations from four key basins of the North Atlantic Ocean to

establish the vertical structure and DVM amplitude to assess the animal-mediated vertical connectivity across these basins. While previous studies have described patterns in mesopelagic acoustic scattering across these 4 basins (e.g. for instance Magnússon, 1996, Dale et al., 1999; Anderson et al., 2005; Pepin, 2013; Norheim et al., 2016), we are unaware of any studies comparing the patterns of vertical distribution and vertical migrations across these 4 basins. Furthermore, we investigate to what extent these patterns are related to environmental variables including the optical environment.

2. Methods

Data were collected in the period May 3rd to June 13th, 2013, during transit and at dedicated stations along the cruise track of RV G.O. Sars (Fig. 1).

2.1. CTD

A Seabird SBE 9 conductivity, temperature and depth probe (CTD) equipped with a rosette with Niskin bottles was used to sample additional environmental parameters. The Niskin bottles provided water samples for analysis of nutrients (nitrite, nitrate, phosphate and silicate) levels, and from selected depths water was also filtered to analyse chlorophyll levels. In addition to the standard temperature, conductivity and pressure sensors, the CTD was also equipped with electronic fluorescence (Chelsea Aquatracka III), oxygen (SBE 43) and PAR (Biospherical/Licor) sensors. The deployment of the PAR sensor was dependent on depth of deployment, standard deployments of the CTD were from 0 to 1000 m, but frequently the CTD was deployed all the way to the bottom. Since the fluorescence sensor on the Seabird CTD (Chelsea Aquatracka III Fluorometer) was not calibrated prior to the cruise, we calibrated the fluorescence measurements using chlorophyll a from Niskin water bottle samples (263 ml) filtered using glass fiber filters (Munktell Ø25 mm, pore retention 0.7 μm) that were stored at −20 °C until acetone extraction and analysis on shore. We did this by comparing measured Chl a in water samples from discrete depths with fluorescence measurements from the sensor, allowing fluorescence measurements to be collected ±2 m from the chlorophyll measurement (on the downcast, water samples were collected on the upcast), at the same geographical position. A linear regression (model type 2, assuming measurement error in both predictor and response variables) was then fit after log-transforming the fluorescence and Chl a values, this regression equation was later used in converting fluorescence measurements to chlorophyll concentrations.

2.2. Underway measurements

A Vaisala MILOS 520 Weather station recorded data on wind speed and direction, air temperature, and atmospheric pressure every 10 min. Deck irradiance (PAR, photosynthetically active radiation) was measured with a PAR LITE sensor (Kipp & Zonen; www.kippzonen.com)
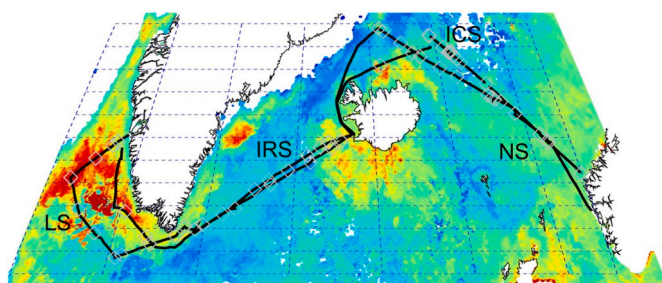

Fig. 1. Cruise track overlayed on satellite derived Chlorophyll a values for May 2013. The cruise covered areas of the Norwegian Sea (NS), the Iceland Sea (ICS), the Irminger Sea (IRS) and Labrador Sea (LS).

connected to the weather station and were stored every 10 min. In addition a Seabird SBE 21 CTD monitored water from the vessels water intake at 8.5 m depth, continuously recording conductivity, temperature and fluorescence (WET Labs WETstar) along the cruise track.

2.3. Acoustics

Acoustic data were collected with the ships Simrad EK60 echosounder system, with transducers mounted on a drop-keel. A total of 6 frequencies were available, but for this work only data from the hull-mounted 38 kHz transducer is included. For this analysis we used the acoustic data where standard noise-removal algorithms had been run in KORONA (Korneliussen et al., 2006, 2016), including removal of TVG amplified noise and noise spikes from other instruments etc. The data were then scrutinized to remove remaining periods of noise, and 38 kHz data for the water-column down to 950 m was then integrated twice, once at a threshold of −90 dB, and once at a threshold of −60 dB, using a bin-size of 600 s by 5 m vertical, similar to the methodology used in (Knutsen et al., 2017). No attempts were made to classify the scattering components in this dataset, we present only the difference in integrated backscatter at the two thresholds, i.e.:

NASCd = NASC[Thr = −90 dB] – NASC[Thr = −60 dB], In the following we use the term "backscatter" to refer to this quantity. This quantity represents the total backscatter added between the 2 thresholds, and we processed the data in this way in order to exclude echoes from schooling epipelagic fish. The results are presented as Nautical Area Scattering coefficients (NASCd, m^2 nmi^{-2}), or converted into mean volume backscattering strengths for the bins for presentation in echograms. Data were split into day and night. In order for this analysis to contain as many days as possible, we defined daytime and nighttime periods on the basis of sun altitude, with data defined as daytime when the sun was more than 6° above the horizon. The cruise spanned ~60 degrees of longitude, and ~10 degrees of latitude during the northern summer. Nighttime data was accepted as time bins where the sun was below the horizon. In order to make the timing comparable between different areas we use apparent solar time in some of the analyses. At apparent time, solar noon occurs at 12:00.

Following (Klevjer et al., 2016) we assessed the amount of backscatter migrating from mesopelagic depths to the epipelagic in each of the four basins. Since water column integrated backscatter (i.e. NASCd) varies horizontally as well as between day and night, we calculated the migrating proportion (MP) from relative rather than from absolute vertical distributions of backscatter. Loss of backscatter from the mesopelagic (in our work "defined" as 200–950 m, following a normally accepted rule of thumb for the upper boundary (Kaartvedt et al., 2019) and the limit of our acoustic data for the lower) during night was interpreted as migration out of that depth range, and the migrating proportion (MP) was estimated as the difference in proportion of water column total backscatter found at mesopelagic depths in paired day-/night samples. The acoustic data from this cruise showed about an order of magnitude reduction in acoustic backscatter assigned to mesopelagic fish from the Norwegian Sea to the Iceland Sea (Klevjer et al., 2019; Table 1), even if the reduction in mesopelagic fish biomass between the areas is not significant (Klevjer et al., 2019, table 2). Acoustic backscatter is often used as a proxy for mesopelagic fish biomass, but the relationship is complex. The most abundant myctophid species in the North Atlantic, *Benthosema glaciale*, may display regression of gas-filled swimbladders for parts of the population (Scoulding et al., 2015). Since gas-filled swimbladders may contribute >90% of the backscattered energy at 38 kHz (Foote, 1980), there may be little correlation between acoustic backscatter and biomass for this species at 38 kHz. In an effort to improve the estimates of the flux of organisms into the upper layers during night, we additionally computed the day to night difference in hull-mounted 120 kHz backscatter in the upper 200 m of the water-column. At this higher frequency, swimbladder resonance is presumably not an issue.

Table 1

Summary of features of backscatter, vertical distribution and DVM, split according to the different basins. Backscatter at 38 kHz are the difference in backscattering between integrations at thresholds of −90 dB and −60 dB. Depth range refers to depth range the different parameters have been measured over. Day/night row indicates whether measurements were taken during day or night. WMD is weighted mean depth of backscatter. Migrating proportion (MP) is calculated as the difference in proportion of backscatter found at mesopelagic depths in paired day/night samples, and migrating backscatter is the product of MP and average daytime mesopelagic backscatter.

	Backscatter 38 kHz	Backscatter 38 kHz	Backscatter 38 kHz	Backscatter 38 kHz	WMD	WMD	MP	Migrating backscatter 38 kHz	Migrating backscatter 120 kHz
Depth range	25–950	25–950	200–950	200–950	25–950	25–950	200–950	200–950	25–200
Day/Night	Day	Night	Day	Night	Day	Night	–	–	–
ICS	66	36	65	33	435	410	0.09	6	0.9
IRS	1310	1099	1292	973	498	463	0.09	112	0.9
LS	741	654	568	394	305	270	0.18	104	−0.1
NS	395	154	377	66	383	211	0.78	293	4.6

Relationships between acoustic based estimates and the hydrographical variables:

We investigated correlations (Pearson product moment correlation) between vertical distribution properties and the measured environmental variables. The distributional variables used were weighted mean depth (day and night), depth of peak scattering (day and night), migration amplitude based both on weighted mean depth and depth of peak scattering, and migrating proportion (MP). The environmental variables were surface salinity, temperature and fluorescence from the underway system, as well as NASC weighted salinity, temperature and oxygen from the CTD profile closest in time. In a first exploratory analysis only salinity came up as significantly correlated (Pearson correlation, Table SI 3) to any of our vertical distribution properties, and only surface light came up as significantly correlated to migrating proportion, when tested across the entire dataset (e.g. inter-regionally). The gradients in the hydrographical environment across the North Atlantic are small (at least when compared to what could be expected for a similar distance directly north-south), and our response variable estimates were noisy, with a relatively low number of day-night cycles (18) observed in total. Since this first analysis did not identify any convincing correlations, we focused in on the relationship between the response variables (e.g. vertical distribution and migration) and an environmental variable where our environment data spanned a strong gradient, *in situ* light levels.

2.4. Light measurements and estimation of attenuation coefficients

A TriOS Ramses hyperspectral irradiance sensor was mounted at the ship and registered incoming irradiance every 5 min. A similar hyperspectral sensor was also used to collect vertical profiles of downwelling irradiance, generally deployed as close as possible to solar noon. Unfortunately, we did not have the possibility of obtaining simultaneous measurements with the TriOS surface reference sensor when the vertical profiles were undertaken. Instead, potential fluctuations in surface light during the vertical profiles were estimated by interpolation of light intensities recorded by a deck mounted PAR sensor, and subsurface light intensities were then scaled by surface PAR fluctuations prior to estimation of light extinction coefficients. We utilized light measurements down to a depth of ~250 m. Since these measurements were taken close to noon and at relatively high light intensities, we assume that bioluminescence has minimal influence on the results, though at low light intensities the sensor requires long integration times, and does not allow us to assess the influence of bioluminescence directly.

The TriOS instrument has a spectral resolution of approximately 3.3 nm, and measures light intensities from ~310 to 1150 nm. For our analysis, we initially selected the wavelengths from 350 to 700 nm. Prior to any analysis, light intensities were converted from energy units (mW m^{-2} nm^{-1}) to quantum flux (mol photons m^{-2} s^{-1} nm^{-1}) for each wavelength channel. For each station depth, as well as wavelength (λ),

specific attenuation coefficients ($K_{obs}(\lambda)$, m^{-1}) for downwelling irradiance were determined from the slopes of regression analyses of natural log transformed irradiance versus depth, after scaling the underwater light measurements for variations in surface PAR irradiance during lowering of the radiometer. We assumed that a relative change in PAR, during the underwater measurements, gave rise to the same relative change in the light measurement of all the wavelength channels. The depth specific $K_{obs}(\lambda)$ estimates were based on at least 3 measurements, and measurements spanning at least 2.5 m in the vertical. $K_{obs}(\lambda)$ estimates (i.e. slopes from the regression analyses) with a coefficient of determination lower than 0.9 were considered too uncertain and removed from the dataset. We also filtered out estimates that were less than the estimated attenuation coefficient of pure seawater ($K_w(\lambda)$ from Morel and Maritorena, 2001). Wavelengths higher than ~550 nm and lower than 380 nm provided low coefficients of determination, we therefore truncated our dataset and dealt only with photon fluxes in the spectral region from 400 to 550 nm.

2.5. A proxy model for attenuation

Light extinction is highly dependent on chlorophyll content. In a previous study involving North Atlantic Water and Norwegian Coastal Water (Aksnes, 2015), it was found that the light attenuation also varied with salinity and oxygen levels. In order to assess *in situ* light conditions at times and in areas where we had no underwater light measurements, we derived a proxy, $K_{proxy}(\lambda)$, from *in situ* CTD measurements of chlorophyll a, salinities and oxygen. As a basis for our proxy we used an empirical wavelength specific model developed for Type I waters (Morel and Maritorena (2001)):

$$K_{Morel}(\lambda) = K_w(\lambda) + \chi(\lambda)(Chl)^{e(\lambda)} \tag{1}$$

where $K_w(\lambda)$ is the influence of pure water at wavelength λ and the last term is an empirical fit to the non-linear relationship between attenuation and chlorophyll for each wavelength.

Our $K_{proxy}(\lambda)$ added a variable component, $K_{var}(\lambda)$, which was related to salinity, chlorophyll and oxygen, such that:

$$K_{proxy}(\lambda) = K_{Morel}(\lambda) + K_{var}(\lambda) \tag{2}$$

where

$$K_{var}(\lambda) = Intercept(\lambda) + CChl(\lambda)(Chl)^{e(\lambda)} + CSal(\lambda)\left(1 - \left(\frac{Sal}{35.298}\right)\right) + COx(\lambda)\left(\frac{Ox}{7.1}\right) \tag{3}$$

The relationship between attenuation and chlorophyll is here not linear, and the wavelength specific exponents, $e(\lambda)$, were assumed to follow Morel and Maritorena (2001). Following the reasoning of Aksnes (2015), we assumed that attenuation would be dependent on the degree

of mixing in of freshwater, and scaled salinities by the maximum salinity (35.298) found in the Norwegian Sea. Oxygen was scaled to reflect reduction from highly oxygenated water. We then estimated the four other coefficients, Intercept(λ), CChl(λ), CSal(λ), and COx(λ), of this model by fitting the modelled $K_{proxy}(\lambda)$ to the observed $K_{obs}(\lambda)$ from all stations and depths while using the corresponding observed values of chlorophyll (Chl), salinity (Sal) and oxygen (Ox). We initially wanted to fit 1 empirical model per basin, but mixing high and low chlorophyll data tended to give unrealistically low values of $K_{proxy}(\lambda)$ at low chlorophyll concentrations. We therefore split the dataset at an arbitrary value of 0.25 mg Chlorophyll a m^{-3}. The reduced amount of data per basin forced us to pool the measurements from low chlorophyll environments into 2 regions, an eastern region containing the Norwegian and Iceland Seas, and a western region consisting of Irminger and Labrador Seas. In instances where the results still were based on regressions of fewer than 20 datapoints, we estimated parameters using the results of a global (i.e. all regions combined) regression. For the eastern regions there were few datapoints also at the high levels of chlorophyll, so data for the Norwegian and Iceland seas were pooled also for high ($>$0.25 mg Chlorophyll a m^{-3}) chlorophyll concentrations.

The proxy model (Eqs. (1) and (2)) was used to approximate underwater irradiance (E(z)) in the wavelength band 400–550 nm from the continuously measured surface irradiance and the salinity and fluorescence measurements from CTD casts:

$$E(z) = F * \sum_{\lambda=400}^{550} E_0(\lambda)* \exp\left(-\int_0^z K_{\rho rox}(\lambda, \sigma)d\sigma\right) \qquad (4)$$

where $E_0(\lambda)$ is measured surface light at wavelength λ. The exponential expression of Eq. (4) calculates the attenuation between surface and depth z. F is a factor correcting for reflection of light in the air-water interface, based on local height of sun. We used formulas from Kirk (1994) to model this, and in this formula reduced the total modelled reflectance by 25% to reflect that we in general had rough water surfaces. In order to assess overall goodness of fit of the output from the model, we compared output from the proxy model (Eq. (4)) with measured photon flux for the band 400–550 nm at the stations where we had data available. Since the input data for the proxy model estimates did not overlap in time with the measurements, both estimated and measured photon fluxes were normalized by levels estimated or measured at 50 m. The depth of 50 m for normalization was chosen partially to minimize potential effects of ship-shadows and wave-focusing of light (Silveira et al., 2014), and partially because we primarily are interested in irradiances in deep waters anyway. Root-mean-square (rms) errors were then calculated as the deviations between the model estimated and the measured photon flux (deeper than 50 m), normalized by the absolute (normalized) measured value, and reported in percent. We additionally report Pearson correlations (R) between log10 transformed estimates and measurements deeper than 50 m.

2.6. Assessing light available to organisms at depth

Using spectrally resolved surface light, the empirical models for $K_{obs}(\lambda)$ and results from CTD casts, we estimated light levels (by use of Eq. (4)) for all 600 s intervals by 5-m vertical bins, which corresponded to the resolution of the acoustic analysis. The resulting irradiance matrix (depth and time) estimate the total ambient irradiance of the acoustic scatterers (also represented in depth and time). The visual pigments of the mesopelagic organisms however also have absorption coefficients that vary with the wavelength of the light, the light actually available to the animals depends on the spectral overlap of the visual pigments with the total ambient light level. Myctophids were an important component of the mesopelagic micronekton in all the basins (Klevjer et al., 2019), and probably are a major component of the scattering layers. In order to

assess light levels available to mesopelagic organisms we used myctophids as a model organism, and further convolved total ambient irradiances with a model of myctophid visual pigment spectral response following Turner et al. (2009). Myctophids typically have absorption maxima in the region 480–492 nm (Turner et al., 2009). We followed the parameterizations used in Turner et al., (2009), using a wavelength of maximum absorption of 480 nm, and report the resulting unit as "myctophid lux" (mylux), which is spectral photon catch rate of an area of a myctophid retina, in µmol photons m^{-2} s^{-1}.

3. Results

To simplify comparison of the environmental variables with the acoustical data, we present vertical profiles showing median values per 1 m depth strata for each basin (Fig. 2). In general, environmental conditions in deeper strata were similar for NS and ICS, and for IRS and LS, though conditions at shallow depths were different. Deep waters in NS and ICS had temperatures of $\sim$ -0.5 °C and salinities greater than 34.9 PSU, whereas deep waters in IRS and LS had temperatures approaching 4 °C. In NS, ICS and IRS temperatures increased towards the surface, whereas LS was characterized by fresher and colder temperatures towards the surface (Fig. 2). In ICS and particularly LS salinities also decreased towards the surface. Oxygen levels were above 6 mL L^{-1} in all basins, down to a depth of 1000 m (Fig. 2).

3.1. In situ light levels and the proxy model

The results of the proxy model for the photon flux in the 400–550 nm band is given in Fig. 3, with full parameter sets and individual goodness of fit values per area, chlorophyll level and wavelength given in the supplementary information (Table SI 1,2). The light profile measurements and CTD casts, which formed the basis for the empirical model, were not concurrent. Both datasets were therefore normalized with respect to irradiance levels at 50 m depth. For most of the stations, the results of the proxy model reproduces general patterns in the attenuation of measured *in situ* irradiance levels reasonably well (Fig. 3, Fig. SI 1). Deeper than 50 m the Pearson correlation between log10 transformed measured and estimated irradiances ranged from 0.83 to 0.98, with root-mean-squared errors in the range 9–213%, suggesting that even if the model manages to account for most of the variability in light levels with depth, some unexplained variation remains.

Light at depth is often estimated through total (i.e. wavelength integrated) irradiances, but the spectral distribution of the available light affects what is actually available to the organisms. Fig. 4 shows measured spectral distribution at depths where the integrated light intensity for the 4 basins were approximately equal, along with the modelled spectral sensitivity of a myctophid with maximum sensitivity at 487 nm. Based on this model (Turner et al., 2009), for the given light intensity range, the ratio of "myctophid" available (e.g. mylux) to total irradiance varies from 26% (LS) to 78% (ICS).

3.2. Vertical distribution and diel vertical migration

Total backscattering levels (NASC) varied between the areas with the highest daytime levels found in IRS (1310 m^2 nmi^{-2}) and the lowest in ICS (66 m^2 nmi^{-2}) (Table 1), with LS (741 m^2 nmi^{-2}) and NS (395 m^2 nmi^{-2}) at intermediate levels. Most of the backscatter (e.g. 38 kHz backscatter difference, see methods) originated from mesopelagic depths (e.g. here defined as 200–950 m) during daytime (ICS 99%, IRS 99%, LS 77%, NS 95%). During daytime the weighted mean depth of average backscatter was shallowest in LS, followed by NS and ICS (Figs. 5, 6, Table 1), with IRS having the deepest distribution. The LS data (Figs. 5, 6) show a relatively shallow center of distribution of daytime 38 kHz backscatter, with the upper edge of the scattering layer found shallower than 200 m throughout the diel cycle. The presence of a weak non-migrating layer at ~700 m depth coincides with the
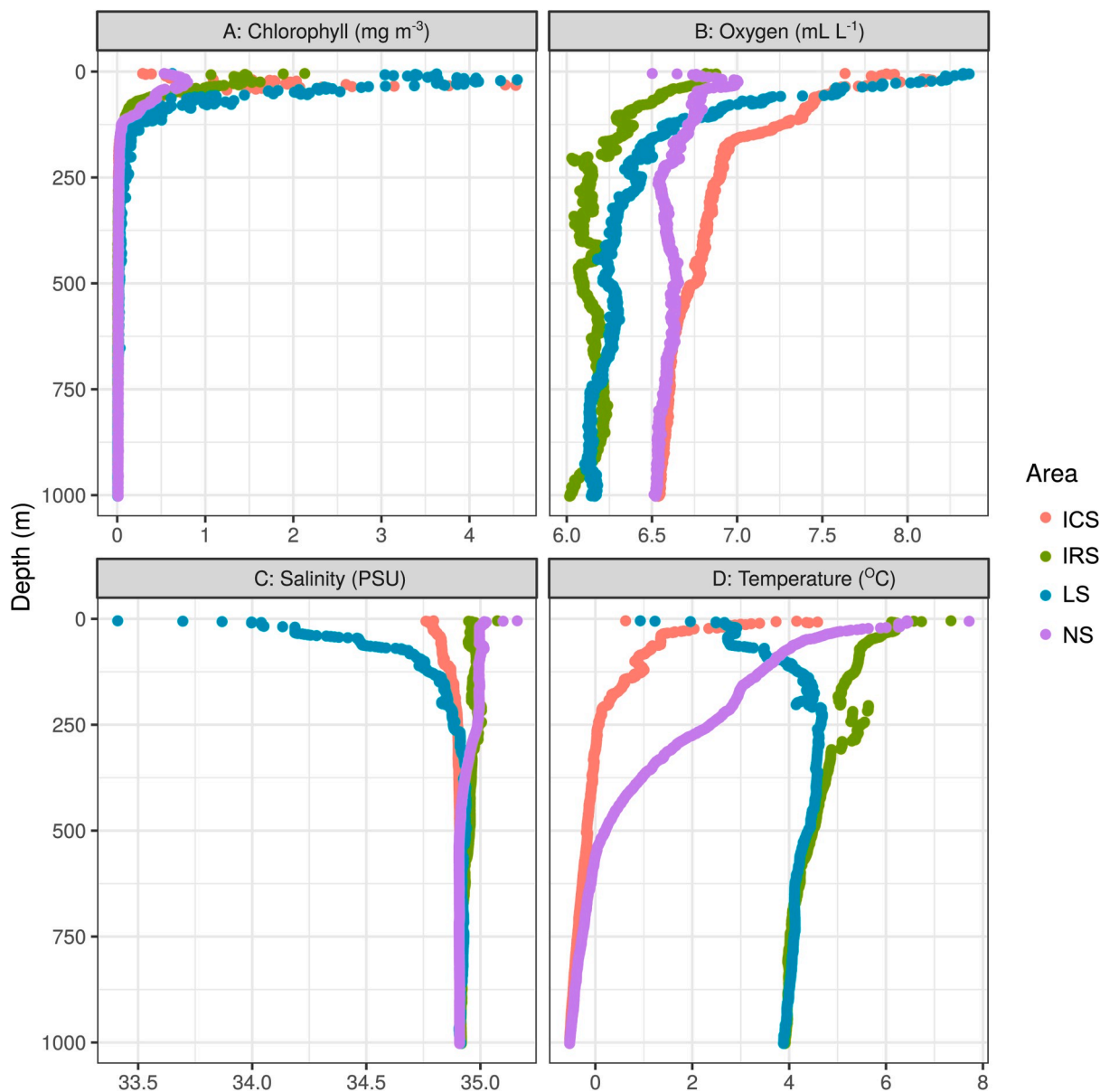
Fig. 2. Hydrographical vertical profiles per basin, based on median values per depth range.

approximate depth of the lower edge of the scattering layer in IRS (Fig. 5). In both NS and ICS only small amounts of 38 kHz backscatter occurred below ~600 m regardless of time of day.

In all areas weighted mean depths (WMD) shifted upwards during night (Table 1), but the magnitude of the upwards shift in WMD varied. Diel variations in WMD were most pronounced in the NS (172 m), with much lower values estimated in LS (35 m) and IRS (35 m) and the ICS (25 m). In both NS and ICS the diel vertical migrations (DVM) appear to include a high proportion of the total 38 kHz backscatter, but very little of this migrating backscatter in ICS actually reaches 200 m (Figs. 5, 6). In IRS and LS only a proportion of the 38 kHz backscatter appears to shift upwards during nighttime (Figs. 5, 6). Migrating proportion from the mesopelagial (MP) estimated from the 38 kHz data therefore varied between the areas, with an estimated 9% of backscatter migrating in IRS and ICS, 18% in LS, and 78% in NS. The estimated backscatter flux at 38 kHz from mesopelagic to the epipelagic depths therefore actually peaked in the NS (migrating NASC: 293 m^2 nmi^{-2}), was lowest in the ICS (6 m^2 nmi^{-2}) and was reasonably similar in ICS and LS (respectively, 112 and 104 m^2 nmi^{-2}).

The 120 kHz backscatter flux, estimated from the diel changes in

backscatter in the upper 200 m, showed a high variability in the paired day-night samples (mean NASC night to day difference/standard deviation in NASC difference, in units of m^2 nmi^{-2}), with the lowest estimated flux into the upper 200 m in the Labrador Sea (−0.1/1.4), very similar results for Irminger Sea (0.9/1) and Iceland Sea (0.9/1.6), and slightly higher values in the Norwegian Sea (4.6/5.1).

For all areas daytime peak backscattering levels were found between the $1.3*10^{-7}$ and $8*10^{-8}$ µmol m^{-2} s^{-1} mylux, and for ICS more than 50% of the backscatter were found within those same light levels (Fig. 6). In all 4 areas nighttime peaks of backscattering are also close to the same light levels. In the NS the daytime distribution has an additional peak at higher light intensities (Fig. 6), but 50% of backscatter was found at light intensities lower than ~10^{-6} µmol m^{-2} s^{-1} mylux (Fig. 6). There are hints of bimodality also in the IRS distribution (Fig. 6), in both these cases the echograms suggests the presence of an additional scattering layer separated from the main layer (Fig. 5). While peak backscatter in LS occurs at light intensities similar to the other areas, the distribution is wide, and has more backscatter at lower light intensities compared with the other areas (Fig. 6).

The daytime irradiance for the mesopelagic scattering layers,
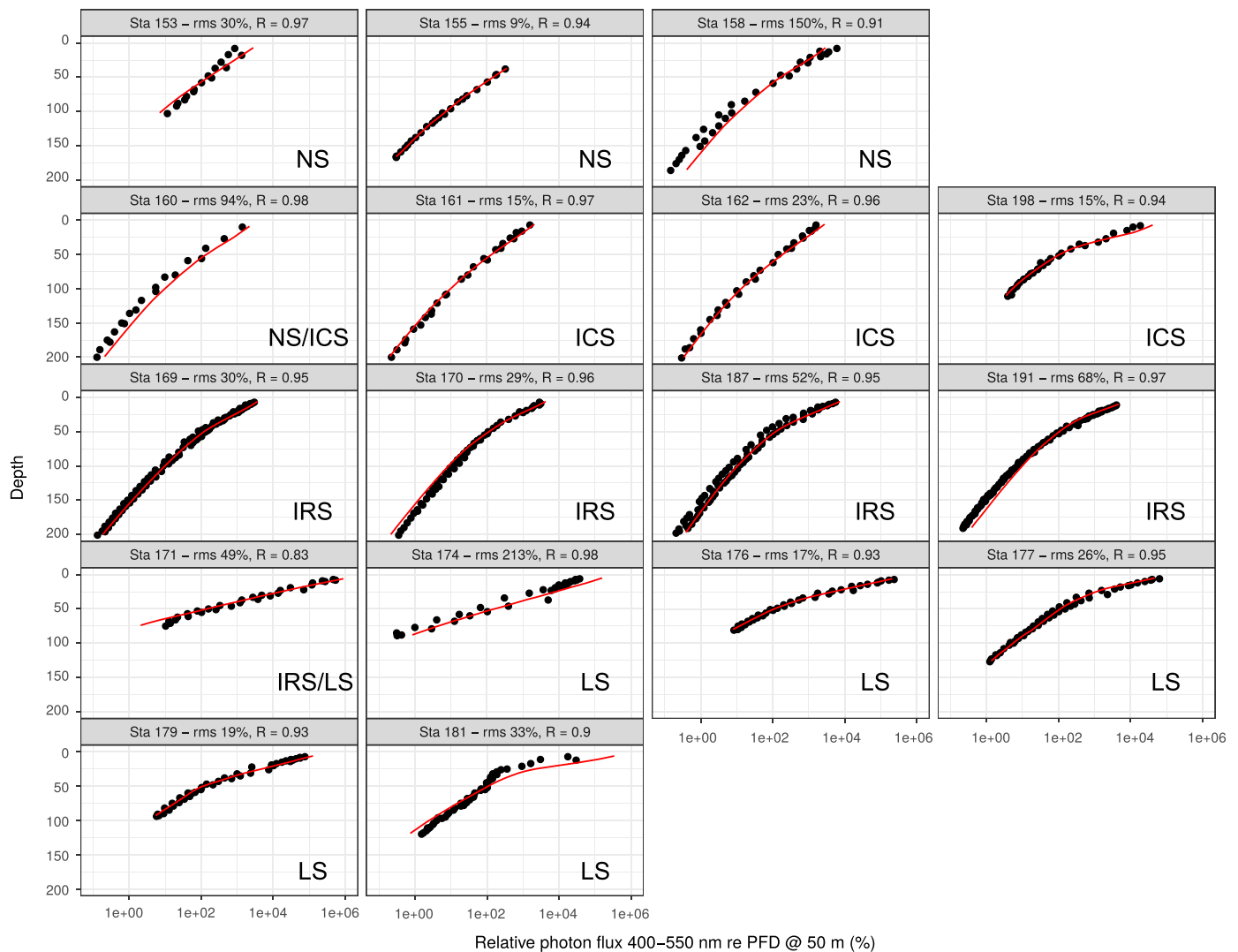
Fig. 3. Measured (black dots) and proxy model estimates (red line) of total photon flux from 400 to 550 nm plotted against depth, for each station with light measurements. Proxy model estimates are based on measured surface light and environmental data from CTD profiles, which did not overlap in time with the underwater measurements, for comparison both measurements and proxy model results were therefore normalized with respect to photon flux levels found at 50 m. Correlations (R) are Pearson correlations between log10 transformed estimates and measurements deeper than 50 m, root-mean-square (rms) errors are deviations between the model estimates and the measurements deeper than 50 m, normalized by the absolute measurement values, and reported in percent. Station 153, 155, 158 are from NS, stations 161, 162, 198 are from ICS, stations 169, 170, 187, 191, are from IRS, stations 171,174, 176, 177, 179, 181 are from LS. CTD stations and light profiles were matched based on time, but were not concurrent. Light profile 160 was from NS, while the corresponding CTD profile was from ICS, light station 171 was from IRS, while the corresponding CTD profile was from LS.

estimated as *in situ* light from the proxy model weighted by a theoretical myctophid eye spectral response, suggests that the migrating mesopelagic layers centered on a narrow range of light intensities, common to all the basins (Fig. 6). In ICS, nocturnal surface light levels were high enough, and *in situ* attenuation (Fig. 3) was low enough, that this "myctophid isolume" never came above 200 m (Figs. 5, 6). Consequently, during the diel vertical migration, only ~10% of backscatter reached the upper ocean (Table 1), in this work defined as the upper 200 m. This despite an apparently high fraction of backscatter migrating upwards in ICS (e.g. Figs. 5, 6). In contrast, the combination of lower nighttime surface light intensities and higher *in situ* attenuation (Figs. 3–5) found just south of the ICS in the NS allowed the "myctophid isolume" to enter the upper 200 m of the ocean, resulting in ~78% of backscatter migrating up from below (Figs. 5, 6). As a result of the combination of the large variation in proportion of backscatter migrating into the upper ocean, as well as a higher mesopelagic backscatter, the backscatter flux between the upper and lower ocean was almost 50 times higher in the NS than in the ICS, which could have

profound impacts for the active flux here. A high proportion of backscatter shifted upwards from its daytime depth in both the NS and ICS (Figs. 5, 6), while in LS and ICS a smaller fraction of the total backscatter appeared to participate in diel migrations. Thus, despite higher total backscattering levels in LS and ICS, estimated 38 kHz backscatter fluxes between the meso- and epipelagic habitats (defined as 200 m depth) were lower than in NS (Table 1).

4. Discussion

Carbon transported by vertically migrating animals form the active component of the biological carbon pump (Turner, 2015 and references therein), therefore understanding the factors that influence vertical migration is essential to understanding the active transport of carbon to depth (Bianchi et al., 2013, 2013b; Klevjer et al., 2016). Studies have reached widely different conclusions when it comes to the relative importance of active flux, with the contribution of zooplankton active transport ranging from 4 to 70% of POC passive flux (Turner, 2015, and
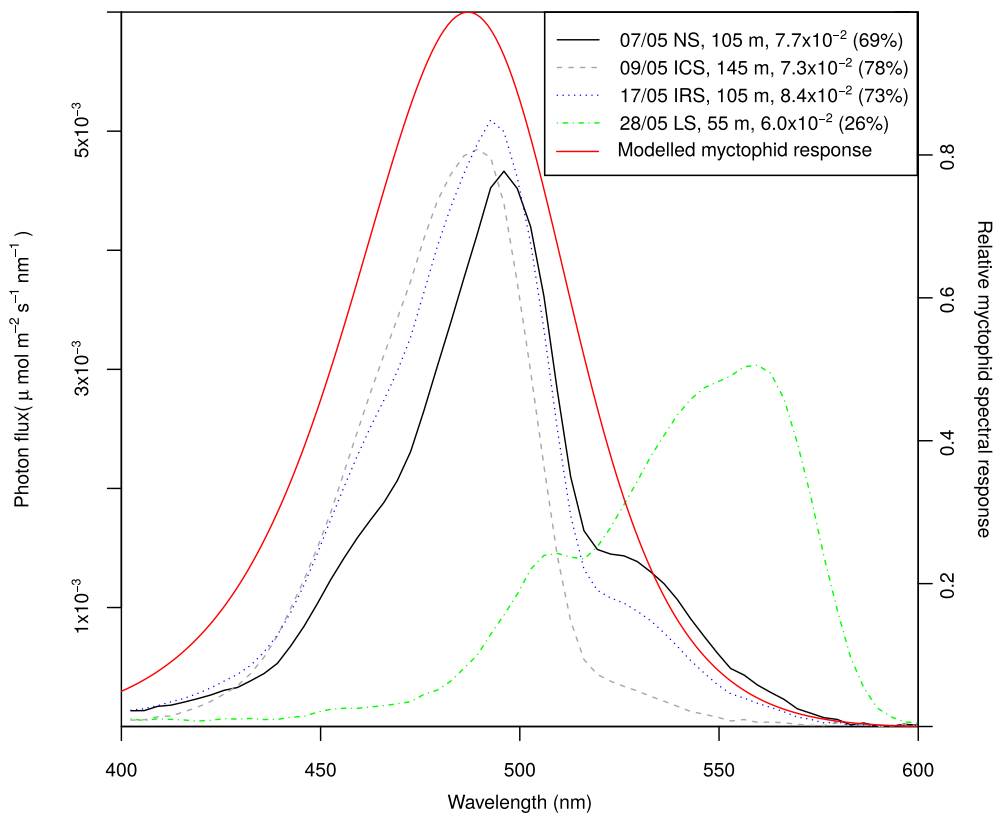
Fig. 4. *In situ* measured irradiance spectra at depths were the integrated light intensity (400–600 nm) in the 4 basins were approximately equal, and modelled myctophid spectral sensitivity (red line) following (Turner et al., 2009). Black line: Spectrum recorded at 105 m depth in NS, total irradiance 7.7×10^{-2} µmol m^{-2} s^{-1}. The ratio (0.69) is the ratio between myctophid lux (i. e. the convolution of *in situ* irradiance and myctophid relative spectral response) (400–600 nm) to total irradiance (400–600 nm). Grey dashed line: Spectrum recorded in ICS as 145 m depth, total irradiance 7.3×10^{-2} µmol m^{-2} s^{-1}, ratio 0.78. Blue dotted line: Spectrum recorded in the IRS at 105 m depth, total irradiance 8.4×10^{-2} µmol m^{-2} s^{-1}, ratio 0.73. Green dash-dotted line: Spectrum recorded in LS, 55 m depth, total irradiance 5.6×10^{-2} µmol m^{-2} s^{-1}, ratio 0.26.

references therein). The contributions of micronekton to active flux has traditionally received less attention, but since biomasses of mesopelagic micronekton are huge (Gjøsæter and Kawaguchi, 1980; Irigoien et al., 2014), and these organisms often show DVM with large amplitudes (Klevjer et al., 2016), the contribution to the active pump is potentially large (Davison et al., 2013).

Since the daytime depth of vertical migrators is an important factor in determining where in the water-column the actively transported carbon is injected, changes in vertical structure will also influence the overall export of carbon from the upper ocean. During the initial phase of applying acoustic methods in scientific studies, several large-scale visualizations of vertical distribution in the oceans were produced (Dickson, 1972; Beklemishev, 1981). The increased focus on the importance of vertical distribution and vertical migratory behaviour of mesopelagic organisms to vertical carbon flux (Davison et al., 2013; Hudson et al., 2014) have led to a renewed interest in such large-scale studies, and also high-lighted the correlation between hydrographic variables and vertical distribution (Bianchi et al., 2013; Irigoien et al., 2014; Klevjer et al., 2016; Béhagle et al., 2016).

While carbon flux to the mesopelagic zone is often studied in the context of carbon sequestration, this carbon flux also represents an important energy input to the mesopelagic ecosystems. The combined flux mediated through vertical migration and passively sinking flux determine how much energy is available to the organisms here, and non-migrating organisms fully depend on energy input from either passively sinking particles (Turner, 2015), from active migrators (Hernandez-Leon et al., 2001; Davison et al., 2013), or from material either subducted or mixed down to mesopelagic depths (Calleja et al., 2019). For the 2 first mechanisms, the energy reaching the mesopelagic has been subject to respiration losses on the way, which will serve to lower the fraction of primary production that is available to mesopelagic organisms. Bacterial metabolism is believed to be the most important energy sink at mesopelagic depths, and the metabolic requirements of other mesopelagic organisms, including at least 1 billion tonnes of mesopelagic fish globally (Gjøsæter and Kawaguchi, 1980), comes in addition to the bacterial metabolic requirements.

The data from this study document large variations in both vertical distributions and proportion and total level of backscatter vertically migrating into the epipelagic across four North Atlantic basins. This implies that the strength of the "micronektonic" active pump varies across these basins. Our results suggest that light levels available at depth had a very strong influence on both the vertical distribution and the proportion of backscatter migrating into the epipelagic zone, highlighting the importance of light in the mesopelagic zone.

4.1. Vertical distribution

On a global scale, which includes hypoxic and anoxic areas, oxygen levels have been found to correlate with both migration amplitude (Bianchi et al., 2013) and migrating proportions (Klevjer et al., 2016) of scattering layers as well as with light penetration (Aksnes et al., 2017). In our study, dissolved oxygen was always higher than 6 mL L^{-1} and effects of oxygen variations are unlikely. Even if distribution and migrations for deep scattering layers have been found to correlate with temperature or temperature differences on a global scale (Bianchi et al., 2013a; Klevjer et al., 2016), the relatively minor gradient across the 4 basins may not have a strong (i.e. detectable in our case) effect. Torgersen et al. (1997) concluded that temperature regimes were likely of minor influence on the vertical structure and migration of Mueller's pearlside in oceanic areas of the NS, and Magnússon (1996) found no influence of temperature on vertical distribution of scattering layers in the IRS. Measures of salinity were correlated with some aspects of mesopelagic distribution and behaviour (Table SI 3), but the salinity measures are likely to be a proxy for watermasses in this case: we are not aware of any ecological studies or theories linking mesopelagic behaviour mechanistically to salinity.

While daytime backscatter originated from a wide depth range across the basins (Fig. 6 A), in terms of estimated light intensities, peak daytime
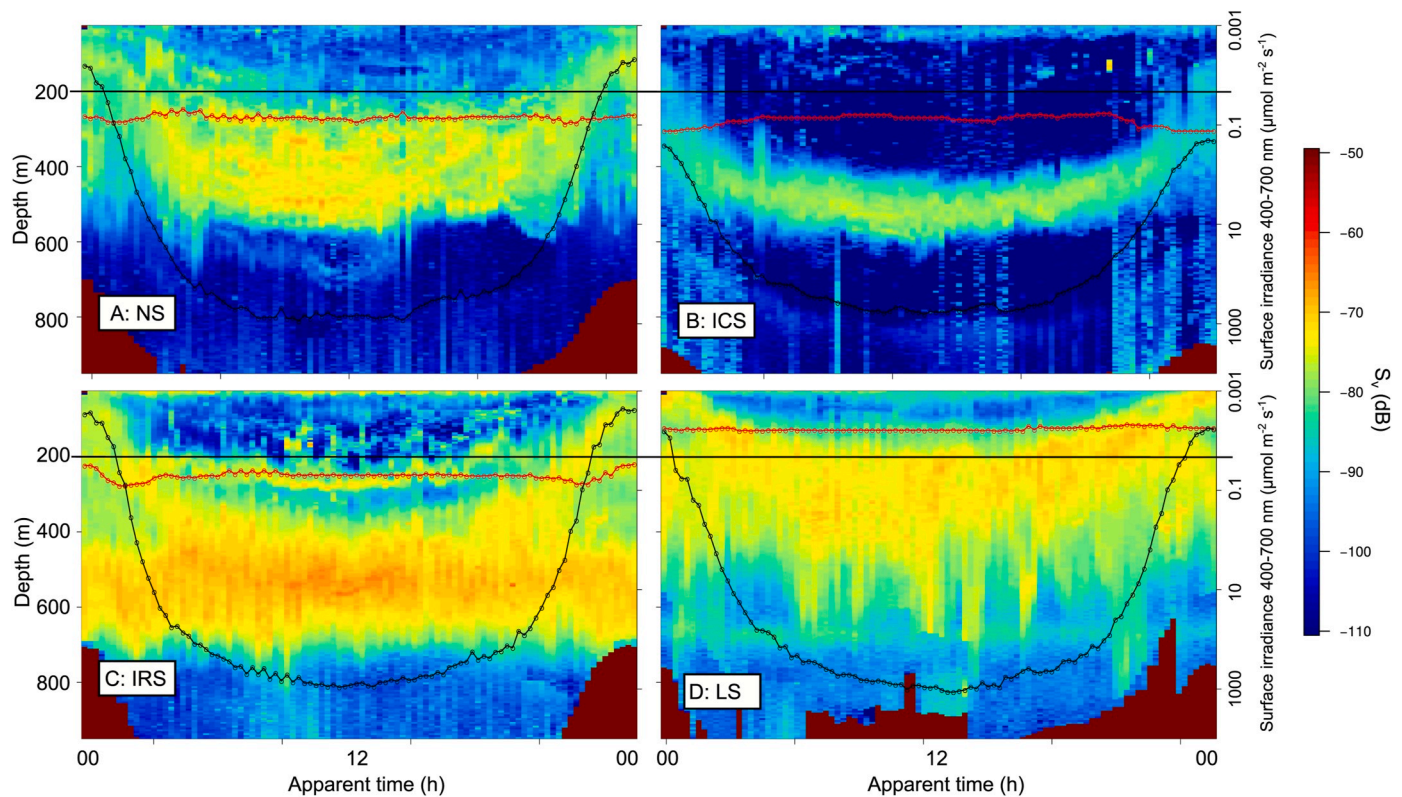
Fig. 5. Echograms of acoustic backscattering difference (38 kHz, s_V@-90 – s_V@-60, see methods), averaged over apparent time (solar noon is at 12:00 apparent time). Panel A shows first crossing of NS, panel B ICS (together covering the period from 04/05/2013 to 12/05/2013), panel C shows first crossing of IRS (from 15/05/2013 to 18/05/2013), while panel D shows second crossing of LS (from 25/05/2013 to 30/05/2013). Black lines and points show the averaged surface irradiance (400–700 nm) measured by the surface reference hyperspectral TriOS sensor (note scale on right hand side), outlining the daily cycle of light variation. Red lines and points indicate the depth of 4.5x Z_{eu} (e.g. Lehodey et al., 2015) for all regions, estimated from the ratio of surface irradiance 400–700 nm and proxy model estimated light at depth (400–550 nm). Black horizontal lines indicate 200 m depth, used to separate meso- and epipelagic zones.

backscatter was found close to the 10^{-7} μmol m^{-2} s^{-1} mylux isolume across all four basins (Fig. 6 B). Similar patterns have recently been reported by Aksnes et al. (2017), who found a correlation between optical properties of water masses and vertical daytime distribution of scattering layers, so that globally distributed scattering layers occupied a relatively narrow range of light intensities (25 and 75 percentiles of mesopelagic backscatter spanned 10^{-6} to 10^{-9} μmol m^{-2} s^{-1} (400–700 nm), Aksnes et al., 2017). This range has been dubbed a mesopelagic "light comfort zone" (LCZ), and emerges if animals actively avoid too high and too low light intensities (Dupont et al., 2009). According to the "antipredation window" hypothesis (Clark and Levy, 1988), such proximate light induced behavior is expected to evolve as a compromise between the need for light to forage, yet avoiding light intensities high enough to let their predators efficiently detect them.

Regardless of the ultimate cause, organisms that swim within a LCZ will perform DVM in synchrony with diel changes in incoming light (Dupont et al., 2009). They are also expected to change vertical position on other time scales, e.g. as consequence of changes in light caused by cloudiness and solar eclipses, or rapid fluctuations in light attenuation (Kaartvedt et al., 2012b). Furthermore, individuals confined to a certain LCZ are expected to distribute shallower along spatial gradients with decreased water column light penetration (e.g. Torgersen et al., 1997).

Peak daytime backscatter across all four basins (Fig. 4) during our cruise was found within a narrow window of light intensities, supporting the hypothesis that daytime vertical distribution follows light-levels, and is strongly correlated with the light attenuation of the water-column above. Euphotic zone depth (Z_{eu}) is sometimes used as a proxy for light at mesopelagic depths (e.g. Lehodey et al., 2015). Satellite estimates of Z_{eu} are readily available and provide large-scale quantifications of *in situ* optical properties. The euphotic zone depth is however

determined by attenuation in the very upper ocean, and the optical conditions here will be more influenced by chlorophyll attenuation than in the deeper watermasses. Extrapolation of Z_{eu} to mesopelagic depths is also problematic as while the light level at Z_{eu} is clearly defined (e.g. 1% of surface light), the light at multiples of Z_{eu} will directly depend on *in situ* diffuse attenuation coefficients. Consequently the light at multiples of Z_{eu} cannot be related to any "general" ratio of surface light. In our data multiples of euphotic zone depth were poor predictors of mesopelagic backscatter distribution (Fig. 6).

Previous studies (e.g. Aksnes et al., 2017) have also had to rely on integrated measures of light intensity to describe mesopelagic scattering layer preferences. In the deep sea, this is relatively unproblematic, since light at depth usually has a narrow spectral distribution, with good overlap with the spectral sensitivity of the mesopelagic organisms (Turner et al., 2009). In other words, at large depths, the spectral composition of the light is determined primarily by the attenuation of water itself, in addition to CDOM components. However, at shallower depth, photosynthetic pigments will modify the spectral composition of the light (Fig. 4), which may decrease the proportion of total light "available" to the organisms. While these effects can be predicted to be minimal deep in the mesopelagic zone, they will be important to organisms migrating vertically into the upper ocean. In our case, whereas ~80% of the total light (400–600 nm) was available to a myctophid at 145 m depth in the ICS, only about 25% was available at 55 m in LS. Previous studies (e.g. Irigoien et al., 2014) have suggested that trophic transfer efficiencies for mesopelagic fish may be higher in oligotrophic waters. Increasing amounts of chlorophyll leads to both increased overall attenuation, and will also lead to decreasing spectral overlap between mesopelagic fish eye sensitivity and *in situ* light, and both these factors decrease the visual range at which a predator can spot a prey
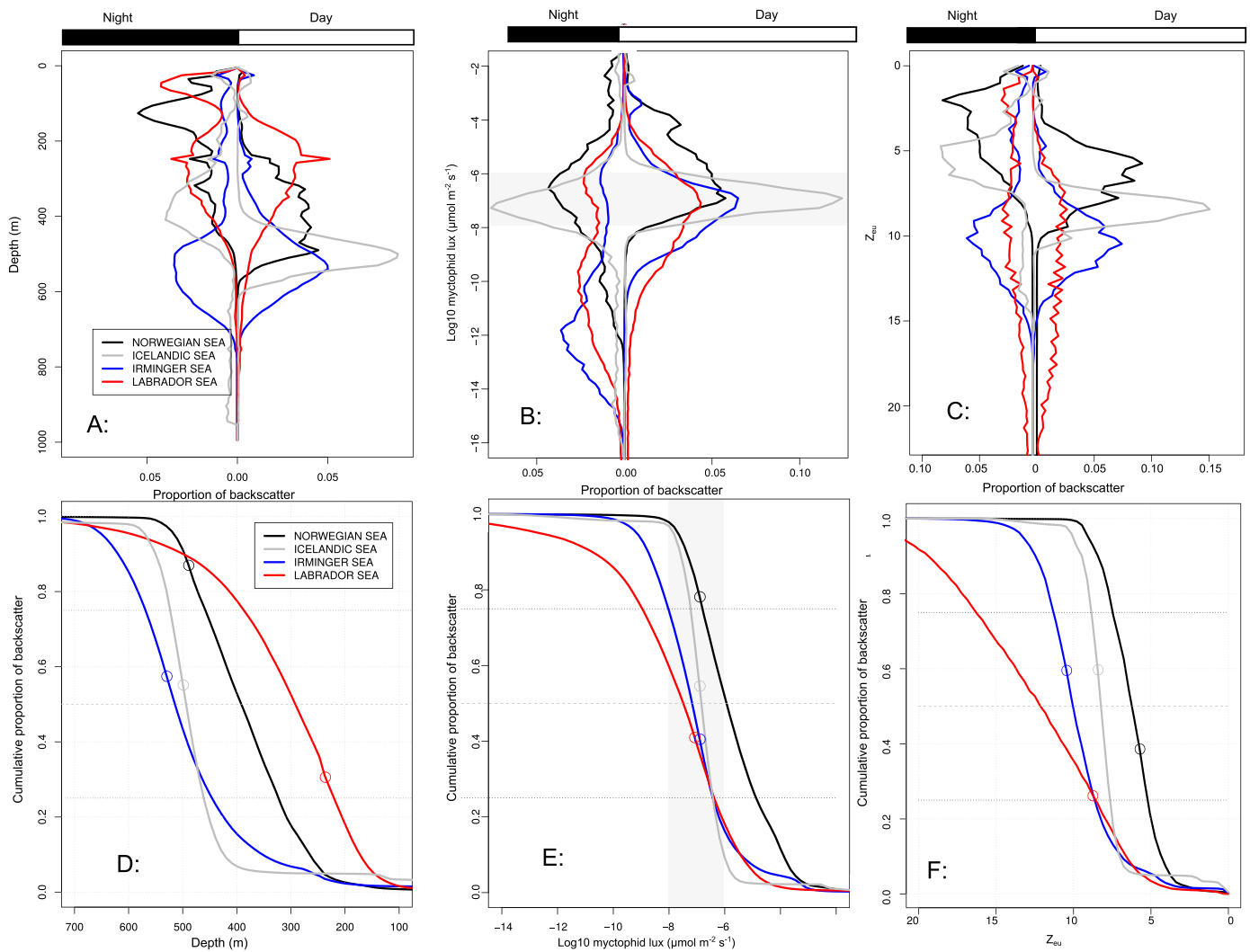
Fig. 6. Details of vertical distribution from the different areas. Left column: Day and night distribution of backscatter as a function of depth. A: Relative backscatter plotted vs. depth for the 4 different areas. D: Cumulative backscatter as a function of depth. Middle column: Daytime distribution of relative backscatter as a function of irradiance levels, in units of myctophid lux (μmol m^{-2} s^{-1}). B: Relative backscatter plotted vs. irradiance levels for the 4 different areas. E: Cumulative relative backscatter as a function of irradiance levels. Right column: Daytime distribution of relative backscatter as a function of multiples of euphotic zone depth, Z_{eu}. Euphotic zone depth was estimated from the ratio of surface irradiance 400–700 nm measured by a hyperspectral TriOS sensor, and proxy model estimated irradiance levels 400–550 nm. C: Relative backscatter plotted vs. multiples of euphotic zone depth for the 4 different areas. F: Cumulative relative backscatter as a function of euphotic zone depth.

based on natural illumination. Increasing chlorophyll levels may correlate with increasing prey densities, but for visual predators this increase may not result in increased encounter rates, due to deterioration of the optical environment.

4.2. Migrating proportion of backscatter

None of the typical oceanographic variables were significantly correlated with the migrating proportion in our case. However, our results suggest that in the ICS, migration into the epipelagic was limited by the levels of nocturnal light (Figs. 5 and 6 and Table 1). It has been previously suggested that the light climate at high latitudes restricts the northward extension of larger populations of mesopelagic fishes (Kaartvedt, 2008), as both the light summer nights and dark winter limits food availability. In a previous study, it was shown that during the Norwegian Euro-Basin cruise nocturnal depths deepened from NS to ICS (Norheim et al., 2016). Depending on the latitude and optical conditions in the watermass, systematic annual patterns in the magnitude of active flux across 200 m can be predicted. While the light summer nights are most pronounced at high latitudes, effects of changes in nocturnal

illumination on migration depths have been reported also from low-latitude systems (Linkowski, 1996; Hernandez-Leon et al., 2002; Hernandez-Leon et al., 2010; Prihartato et al., 2016). Since the light levels perceived by the organisms are controlled by both the surface light and the *in situ* attenuation, optical properties of the water-column modulate the active flux globally.

For the vertically migrating components across the basins, nighttime peak backscatter was also found close to the levels of the daytime peak (Fig. 6), which would be predicted if the animals follow a LCZ. In both LS and ICS a relatively large proportion of the total backscatter remains at depth during night-time, so they are obviously not distributing according to a LCZ. During daytime both migrators and non-migrators are found within the same depth range, and it is not possible to separate these components using hull-mounted acoustics (Figs. 5 and 6). However, the data shows that peak daytime vertical backscatter is found at the same light levels across basins (Fig. 6), regardless of actual depth range. This strongly suggests that at a larger scale, both migrators and non-migrators, distribute according to similar daytime light levels. Similarly, Aksnes et al. (2017) found a strong link between daytime vertical distribution of 38 kHz scattering layers and estimated light

levels in a circumglobal tropical and mid-latitude dataset, but also in their data ~50% of the backscatter remained at depth during night-time (Klevjer et al., 2016). The overall differences in vertical structure and migrations observed between the basins are likely influenced by differences in the species compositions. Myctophids are recognized as an important group among the mesopelagic fishes and are frequently vertical migrators. This group made up virtually all fish biomass in catches from ICS, and 70% in NS, but made up only respectively 50 and 23% of catches in LS and IRS. In IRS Gonostomatids constituted ~30% of the biomass (Klevjer et al., 2019), and this is a group where many of the species are described as non-migratory (Gjøsæter and Kawaguchi, 1980; Olivar et al., 2017). Previous studies have highlighted that the relationship between 38 kHz backscatter and biomass can vary with latitude (Escobar-Flores et al., 2018; Dornan et al., 2019). In these cases decreases in backscatter were not reflected in decreases in biomass. Due to differences in taxonomic and size composition, 1 unit NASC is unlikely to represent the same biomass across our 4 basins (e.g. results in Klevjer et al., 2019). The results from the 120 kHz data are too noisy to draw strong inference on, but they do not contradict the 38 kHz data, and show a marginally higher increase in 120 kHz in the NS.

While taxonomic differences are likely to be important, previous studies of acoustic scattering layers have found pronounced seasonal variation in migration behaviour of mesopelagic fishes normally described as diel migrators, e.g. *Maurolicus muelleri* and *Benthosema glaciale* (Dypvik et al., 2012; Staby et al., 2013). The Norwegian Euro-Basin cruise covered a wide geographic range, making it challenging to separate spatial and temporal patterns. We do not know whether the low migrating proportions observed in LS and IRS represents a typical situation, or whether it is a behavioral feature of short temporal duration. Our data is also not capable of documenting asynchronous migration (Pearre, 2003). If asynchronous migrations are important in these areas, it would serve to increase the vertical transport, but while asynchronous migration of mesopelagic micronekton have been documented in fjords (Kaartvedt et al., 2007, 2008), it has not received enough attention in open ocean environments.

Adherence to a LCZ seems a good fit for the synchronously migrating mesopelagic micronekton, but it falls short when it comes to explaining why both migrating and non-migrating components are found at the same daytime light intensities across the basins. As many "non-migrating" species (e.g. species and individuals not migrating into the epipelagic on a daily basis) are likely to prey on vertical migrators, a vertical shift to track the daytime depth of the vertical migrators seems a reasonable explanation, but we do not have data with the vertical and taxonomic resolution needed to test that hypothesis. Recent modelling studies have addressed the amount of carbon transported by vertically migrating micronekton (Davison et al., 2013; Hudson et al., 2014; Aumont et al., 2018), but a better understanding of the processes influencing both the vertical distributions and the migrations are needed to scale these models realistically to global and annual scales.

Differences in vertically migrating biomasses therefore have direct implications for the transport of energy and carbon to depth. Based on the higher levels of migrating backscatter (Table 1) in the Norwegian Sea, one would expect an overall higher mesopelagic energy input here, if levels of input from primary production are comparable. Mesopelagic secondary production is hard to estimate, but it may be a paradox in our data that IRS and LS have both higher diversity and biomass levels (Klevjer et al., 2019), despite a lower fraction of migrating backscatter. It could be that we missed important processes, source or sink, either due to our limited visit, or it could be that our analysis is not suited to study some of the important processes (e.g. for instance asynchronous migrations).

Our data documents the need for a better understanding of the ecological processes involved. Although the daytime vertical distribution was found to correlate well with estimated *in situ* irradiance levels, and *in situ* light levels could explain differences observed in the migrating flux in the eastern basins, more studies are certainly needed to explain the observed east-west horizontal patterns in both biomasses, diversity and vertical migration.

Declaration of competing interest

The authors declare that they have no known competing financial interests or personal relationships that could have appeared to influence the work reported in this paper.

CRediT authorship contribution statement

Thor A. Klevjer: Conceptualization, Methodology, Investigation, Writing - original draft. **Webjørn Melle:** Funding acquisition, Project administration, Investigation, Writing - original draft. **Tor Knutsen:** Investigation, Writing - original draft. **Dag Lorents Aksnes:** Conceptualization, Investigation, Writing - original draft.

Acknowledgements

Appendix A. Supplementary data

Supplementary data to this article can be found online at https://doi.org/10.1016/j.dsr2.2020.104811.

References

Aksnes, D.L., 2015. Sverdrup critical depth and the role of water clarity in Norwegian Coastal Water. ICES J Mar Sci J Cons 72, 2041–2050.

Aksnes, D.L., Røstad, A., Kaartvedt, S., et al., 2017. Light penetration structures the deep acoustic scattering layers in the global ocean. Sci Adv 3, 2017.

Anderson, C.I.H., Brierley, A.S., Armstrong, F., 2005. Spatio-temporal variability in the distribution of epi- and meso-pelagic acoustic backscatter in the Irminger Sea, North Atlantic, with implications for predation on Calanus finmarchicus. Mar Biol Mar Biol 146, 1177–1188.

Aumont, O., Maury, O., Lefort, S., Bopp, L., 2018. Evaluating the potential impacts of the diurnal vertical migration by marine organisms on marine biogeochemistry. Global Biogeochem. Cycles 32, 1622–1643.

Béhagle, N., Cotté, C., Ryan, T.E., et al., 2016. Acoustic micronektonic distribution is structured by macroscale oceanographic processes across 20–50°S latitudes in the South-Western Indian Ocean. Deep-Sea Res. Part A Oceanogr. Res. Pap. 110, 20–32.

Beklemishev, C.W., 1981. Biological structure of the Pacific Ocean as compared with two other oceans. J. Plankton Res. 3, 531–549.

Bianchi, D., Galbraith, E.D., Carozza, D.A., et al., 2013. Intensification of open-ocean oxygen depletion by vertically migrating animals. Nat. Geosci. 6, 545–548.

Bianchi, D., Stock, C., Galbraith, E.D., Sarmiento, J.L., 2013b. Diel vertical migration: ecological controls and impacts on the biological pump in a one-dimensional ocean model: diel vertical migration impacts. Global Biogeochem. Cycles 27, 478–491.

Calleja, M.L.L., Al-Otaibi, N., Moran, X.A.G., 2019. Dissolved organic carbon contribution to oxygen respiration in the central Red Sea. Sci. Rep. (9), 4690, 2019.

Clark, C.W., Levy, D.A., 1988. Diel vertical migrations by juvenile sockeye salmon and the antipredation window. Am. Nat. 271–290.

Dale, T., Bagoien, E., Melle, W., Kaartvedt, S., 1999. Can predator avoidance explain varying overwintering depth of Calanus in different oceanic water masses? Mar Ecol Prog Ser Mar Ecol Prog Ser 179, 113–121.

Davison, P.C., Checkley Jr., D.M., Koslow, J.A., Barlow, J., 2013. Carbon export mediated by mesopelagic fishes in the northeast Pacific Ocean. Prog. Oceanogr. 116, 14–30.

Dickson, R.R., 1972. On the relationship between ocean transparency and the depth of sonic scattering layers in the North Atlantic. Jaarb. Consum. 34, 416–422.

Dornan, T., Fielding, S., Saunders, R.A., Genner, M.J., 2019. Swimbladder morphology masks Southern Ocean mesopelagic fish biomass. Proc R Soc B Biol Sci 286, 20190353.

Dupont, N., Klevjer, T.A., Kaartvedt, S., Aksnes, D.L., 2009. Diel vertical migration of the deep-water jellyfish Periphylla periphylla simulated as individual responses to absolute light intensity. Limnol. Oceanogr. 54, 1765.

Dypvik, E., Røstad, A., Kaartvedt, S., 2012. Seasonal variations in vertical migration of glacier lanternfish, Benthosema glaciale. Mar. Biol. 159, 1673–1683.

Escobar-Flores, P., O'Driscoll, R., Montgomery, J., 2018. Spatial and temporal distribution patterns of acoustic backscatter in the New Zealand sector of the Southern Ocean. Mar. Ecol. Prog. Ser. 592, 19–35.

Foote, K.G., 1980. Importance of the swimbladder in acoustic scattering by fish: a comparison of gadoid and mackerel target strengths. J. Acoust. Soc. Am. 67, 2084–2089.

Gjøsæter, J., Kawaguchi, K., 1980. A review of the world resources of mesopelagic fish. FAO Fish. Tech. Pap. 193, 1–151.

Hernandez-Leon, S., Almeida, C., Yebra, L., Aristegui, J., 2002. Lunar cycle of zooplankton biomass in subtropical waters: biogeochemical implications. J. Plankton Res. 24, 935–939.

Hernandez-Leon, S., Gomez, M., Pagazaurtundua, M., Portillo-Hahnefeld, A., Montero, I., Almeida, C., 2001. Vertical distribution of zooplankton in Canary Island waters: implications for export flux. Deep-Sea Res. I 48, 1071–1092, 2001.

Hernandez-Leon, S., Franchy, G., Moyano, M., et al., 2010. Carbon sequestration and zooplankton lunar cycles: could we be missing a major component of the biological pump? Limnol. Oceanogr. 55, 2503–2512.

Hudson, J.M., Steinberg, D.K., Sutton, T.T., et al., 2014. Myctophid feeding ecology and carbon transport along the northern Mid-Atlantic Ridge. Deep-Sea Res. Part A Oceanogr. Res. Pap. 93, 104–116.

Irigoien, X., Klevjer, T.A., Røstad, A., et al., 2014. Large mesopelagic fishes biomass and trophic efficiency in the open ocean. Nat. Commun. 5, 3271.

Kaartvedt, S., Klevjer, T.A., Torgersen, T., et al., 2007. Diel vertical migration of individual jellyfish (Periphylla periphylla). Limnol. Oceanogr. 52, 975–983.

Kaartvedt, S., 2008. Photoperiod may constrain the effect of global warming in arctic marine systems. J. Plankton Res. 30, 1203–1206.

Kaartvedt, S., Torgersen, T., Klevjer, T.A., et al., 2008. Behavior of individual mesopelagic fish in acoustic scattering layers of Norwegian fjords. Mar. Ecol.: Prog. Ser. 360, 201–209.

Kaartvedt, S., Staby, A., Aksnes, D.L., 2012. Efficient trawl avoidance by mesopelagic fishes causes large underestimation of their biomass. Mar. Ecol. Prog. Ser. 456, 1–6.

Kaartvedt, S., Klevjer, T., Aksnes, D., 2012b. Internal wave-mediated shading causes frequent vertical migrations in fishes. Mar. Ecol. Prog. Ser. 452, 1–10.

Kaartvedt, S., Langbehn, T.J., Aksnes, D.L., 2019. Enlightening the ocean's twilight zone. ICES J. Mar. Sci. 76 (4), 803–812.

Kampa, E.M., 1971. Photoenvironment and sonic scattering. In: Farquhar, G.B., Washington, D.C. (Eds.), Proceedings of an International Symposium on Biological Sound-Scattering in the Ocean. Maury Center for Oceanic Science, pp. 51–59. Rep. MC-005.

Kirk, J.T.O., 1994. Light and Photosynthesis in Aquatic Ecosystems. Cambridge University Press, p. 509.

Klevjer, T.A., Irigoien, X., Røstad, A., et al., 2016. Large scale patterns in vertical distribution and behaviour of mesopelagic scattering layers. Sci. Rep. 6, 19873.

Klevjer, T., Melle, W., Knutsen, T., Strand, E., Korneliussen, R., Dupont, N., Salvanes, A. G.V., Wiebe, P.H., 2019/This volume. Micronekton biomass distribution, improved estimates across four north Atlantic basins. Deep Sea Research II (in press).

Knutsen, T., Wiebe, P.H., Gjøsæter, H., et al., 2017. High latitude epipelagic and mesopelagic scattering layers—a reference for future arctic ecosystem change. Front Mar Sci 4, 334.

Korneliussen, R., Ona, E., Eliassen, I., et al., 2006. The large scale survey system–LSSS. In: Proceedings of the 29th Scandinavian Symposium on Physical Acoustics. Ustaoset.

Korneliussen, R.J., Heggelund, Y., Macaulay, G.J., et al., 2016. Acoustic identification of marine species using a feature library. Methods Oceanogr 17, 187–205.

Lehodey, P., Conchon, A., Senina, I., et al., 2015. Optimization of a micronekton model with acoustic data. ICES J. Mar. Sci. 72, 1399–1412.

Linkowski, T.B., 1996. Lunar rhythms of vertical migrations coded in otolith microstructure of North Atlantic lanternfishes, genus Hygophum (Myctophidae). Mar. Biol. 124, 495–508.

Longhurst, A.R., Glen Harrison, W., 1989. The biological pump: profiles of plankton production and consumption in the upper ocean. Prog. Oceanogr. 22, 47–123.

Magnússon, J., 1996. The deep scattering layers in the Irminger Sea. J. Fish. Biol. 49, 182–191.

Morel, A., Maritorena, S., 2001. Bio-optical properties of oceanic waters: a reappraisal. J Geophys Res Oceans 106, 7163–7180.

Norheim, E., Klevjer, T., Aksnes, D., 2016. Evidence for light-controlled migration amplitude of a sound scattering layer in the Norwegian Sea. Mar. Ecol. Prog. Ser. 551, 45–52.

Olivar, M.P., Hulley, P.A., Castellón, A., et al., 2017. Mesopelagic fishes across the tropical and equatorial Atlantic: biogeographical and vertical patterns. Prog. Oceanogr. 151, 116–137.

Pearre, S.J., 2003. Eat and run? The hunger/satiation hypothesis in vertical migration: history, evidence and consequences. Biol. Rev. Camb. Phil. Soc. 78, 1–79.

Pepin, P., 2013. Distribution and feeding of Benthosema glaciale in the western Labrador Sea: fish–zooplankton interaction and the consequence to calanoid copepod populations. Deep-Sea Res. Part A Oceanogr. Res. Pap. 75, 119–134.

Prihartato, P., Irigoien, X., Genton, M., Kaartvedt, S., 2016. Global effects of moon phase on nocturnal acoustic scattering layers. Mar. Ecol. Prog. Ser. 544, 65–75.

Proud, R., Handegard, N.O., Kloser, R.J., et al., 2018. From siphonophores to deep scattering layers: uncertainty ranges for the estimation of global mesopelagic fish biomass. ICES J. Mar. Sci. 76 (3), 718–733.

Scoulding, B., Chu, D., Ona, E., Fernandes, PaulG., 2015. Target strengths of two abundant mesopelagic fish species. J. Acoust. Soc. Am. 137, 989–1000.

Steinberg, D.K., Carlson, C.A., Bates, N.R., et al., 2000. Zooplankton vertical migration and the active transport of dissolved organic and inorganic carbon in the Sargasso Sea. Deep-Sea Res. Part A Oceanogr. Res. Pap. 47, 137–158.

Silveira, N., Suresh, T., Talaulikar, M., et al., 2014. Sources of errors in the measurements of underwater profiling radiometer. Indian J. Mar. Sci. 43 (1), 88–95.

Staby, A., Srisomwong, J., Rosland, R., 2013. Variation in DVM behaviour of juvenile and adult pearlside (Maurolicus muelleri) linked to feeding strategies and related predation risk. Fish. Oceanogr. 22, 90–101.

Sutton, T.T., 2013. Vertical ecology of the pelagic ocean: classical patterns and new perspectives. J. Fish. Biol. 83, 1508–1527.

Torgersen, T., Kaartvedt, S., Melle, W., Knutsen, T., 1997. Large scale distribution of acoustical scattering layers at the Norwegian continental shelf and the Eastern Norwegian Sea. Sarsia 82, 87–96.

Turner, J.R., White, E.M., Collins, M.A., et al., 2009. Vision in lanternfish (Myctophidae): adaptations for viewing bioluminescence in the deep-sea. Deep-Sea Res. Part A Oceanogr. Res. Pap. 56, 1003–1017.

Turner, J.T., 2015. Zooplankton fecal pellets, marine snow, phytodetritus and the ocean's biological pump. Prog. Oceanogr. 130, 205–248.

Widder, E.A., Caimi, F.M., Taylor, L.D., Tusting, R., 1992. Design and development of an autocalibrating radiometer for deep sea biooptical studies,. In: Proceedings of OCEANS '92, Mastering the Oceans through Technology, pp. 525–530. IEEE.